

# Influence of the hydrogenation on the physical properties of Si-doped ZnO films in the application of transparent conducting oxides

A. A. DAKHEL\*

*Department of Physics, College of Science, University of Bahrain, P.O. Box 32038, Sakhir, Kingdom of Bahrain*

ZnO doped with different amounts of Si ions (ZnO: Si) nano-composite films deposited on glass substrates has been prepared by vapor deposition technique. The influences of Si-doping on the structural and optical properties have been studied. The crystalline structure was gradually deteriorated by increasing the Si- contents. The prepared films were annealed in a hydrogen atmosphere to study the effects on the properties. It was found that the hydrogenation accelerated the crystalline disorder. The conduction parameters were concluded. The carrier concentration of the host ZnO was increased by ~ 46 % by increasing the Si- content by ~ 4.7at %.

(Received March 3, 2021; accepted February 11, 2022)

*Keywords:* Si-doped zinc oxide, ZnO thin films, Hydrogenation

## 1. Introduction

Zinc oxide (ZnO) belongs to the group of transparent conducting oxides (TCOs). It is a degenerate semiconductor of a direct wide optical band gap (~ 3.3 eV) and transparent properties in the visible region [1-3]. The natural non-stoichiometric structure and intrinsic structural point defects like oxygen vacancies ( $V_O$ ) and zinc interstitials ( $Zn_i$ ) stand behind its transparent conducting properties [2]. ZnO has drawn great attention due to numerous practical applications including solar-cell technologies, smart windows, and various wide-range of optoelectronic devices including transparent thin-film transistors, photo-detectors, light-emitting diodes, and laser diodes [4,5]. The fundamental TCO properties of ZnO can be controlled by doping with different types of ions [6-9]. The dopant in the present investigation was silicon ions. Thus, the present work is aimed to prepare and study Si-integrated ZnO (ZnO:Si) nano-crystallite thin films by using a physical vapor deposition (PVD) method assisted by a graphite fine powder as a temperature reducing agent. Moreover, annealing in a hydrogen atmosphere (hydrogenation) was employed to homogenize the distribution of the Si dopant throughout the ZnO lattice. Furthermore, the hydrogenation should increase the carrier concentration and create additional oxygen vacancies.

## 2. Experimental procedure

ZnO:Si thin films were deposited on Corning glass substrates cleaned by acetone and deionized water under sonication. The starting materials were ZnO and SiO monoxides (from Aldrich Chemicals Inc). It was known that the physical vapor deposition (PVD) technique has been widely used for the deposition of nanostructured ZnO

films. Moreover, graphite (C) fine-powder was used as an evaporation temperature reducing agent (TRA) that can reduce the evaporation temperature by obtaining nanograins [10-12]. Therefore, ZnO and carbon fine powder (mass ratio: 1:1) were well mixed together with a certain controlled amount of fine SiO-powder and then pelletized. The calculated Si content of the (Si/Zn) of the prepared films were ~ 1.2%, 4.7%, 9.3%, and 14%, which were referred to as ZnSiO-X (where X=1, 2, 3, and 4), respectively. Then a small piece from each pressed-powder sample was thermally evaporated in a vacuum (~  $10^{-6}$  torr) by alumina baskets (Midwest tungsten service, USA). Undoped ZnO film was also prepared by the same procedure, for comparison. The deposited thin films/substrates were annealed in air at 400 °C for 1 h and then slowly cooled in the closed oven to room temperature. Then, the film/substrate samples were annealed in a hydrogen gas atmosphere at 350 °C for 20 min and were referred as ZnSiO-X-H. Thicknesses of the prepared films were measured after annealing by a MP100-M spectrometer (Mission peak optics, USA) to be in the range of 200-240 nm. The crystal structure of the films was studied by the XRD technique using a Rigaku Ultima-VI X-ray diffractometer equipped with PDXL built-in program for Rietveld refinement structural analysis. The optical normal transmittance,  $T(\lambda)$  and reflectance,  $R(\lambda)$  of the films/glass samples were measured in the spectral range (300-1500) nm by a Shimadzu UV-3600 double beam spectrophotometer.

## 3. Structural characterization

Fig. 1a shows the XRD patterns of the pristine and ZnO:Si films/glass substrates. The pristine ZnO film grew in [002] preferred orientation (i.e. the crystallites were preferentially oriented with (002) plane parallel to the

substrate surface) due to the lowest formation energy [13, 14]. The obtained values of lattice parameter ( $c$ ) are close to the standard value for the hexagonal wurtzite ZnO (SG=P6<sub>3</sub>mc);  $a = b = 3.2489 \text{ \AA}$ ,  $c = 5.2062 \text{ \AA}$  (JCPDS 01-07-8070 card).

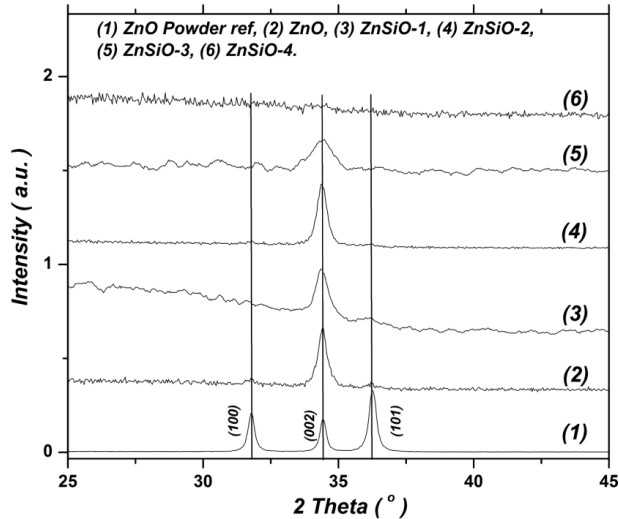


Fig. 1a. X-ray diffraction (XRD) patterns of undoped and Si doped ZnO thin films

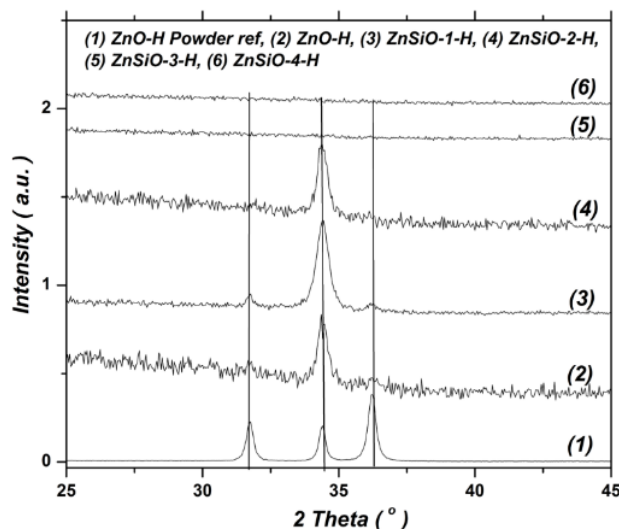


Fig. 1b. X-ray diffraction (XRD) patterns of hydrogenated undoped and Si doped ZnO thin films

However, the crystallinity of ZnO films gradually decreases with the increasing of Si content due to the incorporation Si ions into the ZnO lattice; a similar behaviour was also observed in [15,16]. The lattice-distortion was attributed to the Si, which created structural disorders leading to the amorphization. As observed (Figs.1a-b) ZnO:Si films were transformed totally to amorphous structure with the Si content (%) > 9.3. However, these experimental observations confirmed the Si incorporation into ZnO lattice. Table 1 presents the parameters obtained from the XRD data. The lattice parameter  $c$  was determined from the hexagonal ZnO structure using PDXL built-in program. The lattice parameter  $c$  slightly increases with Si doping level for up to

4.7at% before reduction toward the amorphous structure. The type of silicon incorporation into ZnO lattice could be explained from the geometrical point of view. The ionic radius of Zn<sup>2+</sup>(IV coordination) of ZnO crystal is 0.074 nm, which is much greater than that of dopant Si<sup>4+</sup> 0.026 nm [17] and much less than that of Si atomic radius (0.111 nm). Therefore, the substitution of Zn ions with Si ions, if happened, would strongly disturb the crystalline structure of the host ZnO crystal, according to Hume-Rothery rules. Thus, the substitution of Si<sup>4+</sup> for Zn<sup>2+</sup> ions by the doping process to form a solid solution is unlikely to occur. Hence, the occupations of interstitial locations of ZnO lattice by Si ions (with an oxidation number of less than 4+) were most likely to take place, causing an increase in the observed  $c$ -value. These conclusions were also confirmed by the XPS studies on the chemical state of Si dopant ions in ZnO medium and found that Si ions were being in oxidation states of less than 4+.

Table 1. Bragg angle  $2\theta$ °(002), Lattice parameter ( $c$ ), Scherrer crystallite size (CS) and bandgap ( $E_g$ )

| Sample               | $2\theta$ °(002) | $c$ (Å) | CS(nm) | $E_g$ (eV) |
|----------------------|------------------|---------|--------|------------|
| ZnO                  | 34.42            | 5.206   | 25.0   | 3.22       |
| ZnSiO-1              | 34.38            | 5.210   | 20.1   | 3.23       |
| ZnSiO-2              | 34.34            | 5.216   | 18.7   | 3.24       |
| ZnSiO-3              | 34.44            | 5.208   | 13.0   | 3.24       |
| ZnSiO-4              | amorphous        |         |        | 3.23       |
| Hydrogenated samples |                  |         |        |            |
| ZnO-H                | 34.34            | 5.218   | 19.6   | 3.22       |
| ZnSiO-1-H            | 34.37            | 5.213   | 16.6   | 3.23       |
| ZnSiO-2-H            | 34.30            | 5.224   | 12.7   | 3.24       |
| ZnSiO-3-H            | amorphous        |         |        | 3.24       |
| ZnSiO-4-H            | amorphous        |         |        | 3.23       |

The average crystallite size (CS) was estimated by the known Scherrer formula  $CS = 0.9\lambda / B \cos\theta_B$ , where  $\lambda$  is the X-ray wavelength (1.5418 Å),  $\theta_B$  is the Bragg diffraction peak and  $B$  is the line-width at half maximum (in radians) [13]. The average CS was found to be of nano-size of ~ 25 nm for pristine ZnO and decreased from increasing of Si incorporation level attaining ~ 13 nm for ~9.3at% Si. The residual stress in the thin films can be determined by,  $\sigma = -233[(c-c_0)/c_0]$  GPa [19], where  $c_0 = 0.52066 \text{ nm}$  is the relaxed lattice constant for bulk ZnO [20]. The results were  $\sigma \sim -0.7, -1.9,$  and  $-0.4 \text{ MPa}$  to ZnSiO-1, ZnSiO-2, and ZnSiO-3, respectively (the minus sign refers to compressive stress). The microstructural stress was reduced as the structure going to be the amorphous state.

In the present work, annealing in hydrogen atmosphere was aimed to enhance the distribution of the incorporated Si ion-species throughout the ZnO lattice by tossing. Fig.1b presents the XRD patterns of the hydrogenated pristine and ZnO:Si films/glass substrates. By comparing it with fig.1a, it seems that the hydrogenation did not introduce major structural changes in host ZnO lattice. However, it corroded the crystallites (Table 1) since the H<sub>2</sub> molecules adsorbed into the grains via the crystallite boundaries, will be dissociated into H ion-species under the influence of Si

ions dopant [21]. The formed H ion-species created O-vacancies that corrode the crystallites and slightly increased the parameter  $c$  (Table 1). The destroying of the crystalline structure by the hydrogenation began with Si% content of less than 4.7at%, or the hydrogenation assisted the incorporated Si ions to destroy ZnO crystalline structure. This might be due to the effect of the tossing of Si ions accumulated on grain and crystallite boundaries to enter into ZnO lattice.

#### 4. Optical characterization

Fig. 2a displays the spectral normal transmittance,  $T(\lambda)$  and reflectance,  $R(\lambda)$  of the prepared pristine, and ZnO:Si films/glass samples. The pristine ZnO nanocrystallite film showed almost translucent in the visible (Vis) region and becoming transparent in the NIR spectral region. Moreover, the results show that the overall transparency of the films was improved by Si incorporation. The spectral reflectance,  $R(\lambda)$  of all investigated samples varies in the range of less than 10%. Generally, the increase of Si incorporation caused an increase in spectral  $R(\lambda)$ , especially in the Vis region.

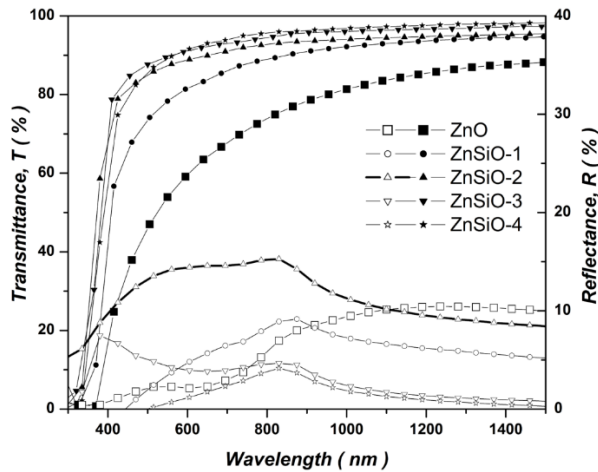


Fig. 2a. Spectral transmittance ( $T(\lambda)$ ) and reflectance ( $R(\lambda)$ ) of pristine and Si doped ZnO thin films

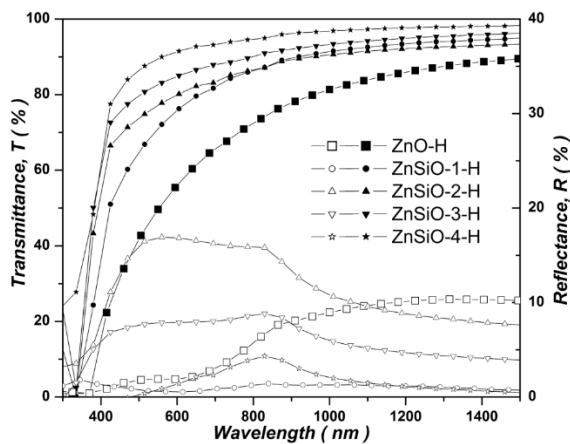


Fig. 2b. Spectral transmittance ( $T(\lambda)$ ) and reflectance ( $R(\lambda)$ ) of hydrogenated pristine and Si doped ZnO thin films

The spectral absorption coefficient  $\alpha(\lambda)$  is related to the absorbance  $A(\lambda)$  by,  $\alpha(\lambda) = A(\lambda)/d$ , where  $d$  is the film thickness and  $\alpha(\lambda)$  can be calculated by  $\alpha(\lambda) = (1/d) \ln[(1-R(\lambda))/T]$ . The direct bandgap  $E_g$  could be found by Tauc technique [22];  $[A(\lambda) E]^2 = B_{op} (E - E_g)$ , where  $E$  is the photon energy and  $B_{op}$  is the film's constant.

The extrapolation of the straight-line portion of the  $(A.E)^2$  vs.  $E$  plot for each film sample, as shown in figs.3a, gives the direct optical band gap ( $E_g$ ). For pristine nanocrystallite ZnO film, the obtained optical bandgap (3.22eV) is consistent with the known experimental range of values; 3.1-3.3 eV for pristine ZnO prepared by different methods [23,24].

The obtained optical band gaps of ZnO:Si listed in Table 1 are slightly broader than that of pristine ZnO film. The inset of Fig.3a illustrates graphically the variation of  $E_g$  with Si% content showing the increasing function for the low Si% before decreasing for higher than 9.3%Si. To explain the reasons behind the bandgap shift, it should first examine the influence of quantum confinement (6) effect. According to Brus [25,26], the QC effect can be determined by the following equation:

$$E_g (eV) \approx E_g^{Bulk} (eV) + \frac{h^2}{8\mu r^2} = E_g^{Bulk} + 1.556/r^2$$

where  $E_g^{Bulk}$  is the bandgap of the bulk ZnO material,  $h$  is the Planck's constant,  $r$  (nm) is the average radius of the nanoparticle measured by XRD/TEM,  $\mu$  is the reduced exciton mass ( $\mu=0.242m_0$  for ZnO [27]). Therefore, the QC effect has a detectable blue-shift effect for very tinny grain sizes (5-10 nm). However, in the present work, the average CS  $\sim$  13-25 nm and the grains are usually larger than crystallites, therefore the obtained experimental blue-shift of the bandgap cannot be explained through QC model. Hence, the blueshift (bandgap widening BGW) should be explained mainly by the Moss-Burstein (B-M) effect [28]. Meanwhile, the decreasing of  $E_g$  (BGN) due to the Si incorporation level higher than  $\sim$ 7at% level would be attributed mainly to the created structural point defects like O-vacancies that could energetically be represented by dopant levels located at the bottom and overlapped with the conduction band of the host ZnO causing a decrease of  $E_g$ . The results show that the hydrogenation of the samples has no considerable effect on the values of the energy gaps, as shown in table 1 and inset of Fig. 3a.

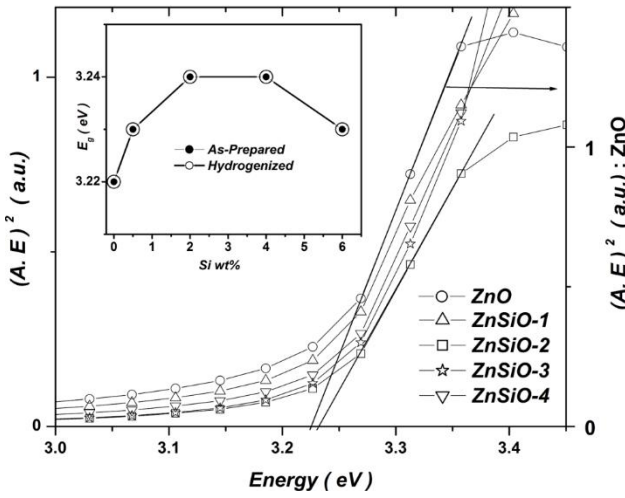


Fig. 3a. Tauc plot for pristine and Si doped ZnO thin films. The inset shows the Si doping level dependence of band gaps for all the samples

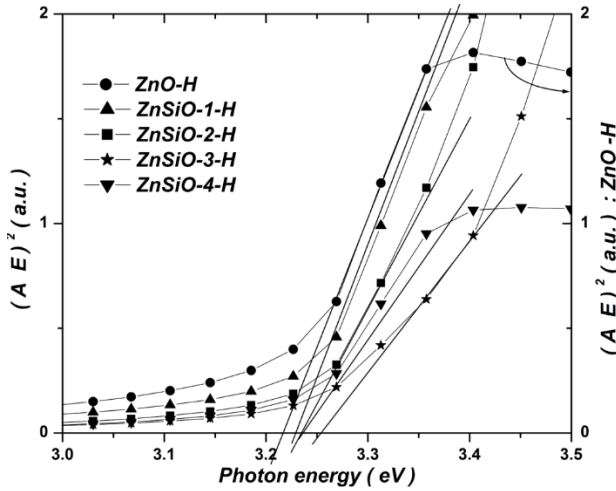


Fig. 3b. Tauc plot for hydrogenated pristine and Si doped ZnO thin films

According to the Moss-Burstein (B-M) model, the shift ( $\Delta E_g^{BM}$ ) of the measured optical bandgap ( $E_g$ ) of the doped degenerate semiconductor concerning its intrinsic bandgap ( $E_g^{int}$ ) is given by;

$$\Delta E_g^{BM} = (E_g - E_g^{int}) = S_{BGW} N_{carr}^{2/3}, S_{BGW} = (\hbar^2 / 2\mu)(3\pi^2)^{2/3} \quad (1)$$

where  $N_{carr}$  is the carrier concentration. For ZnO, the BGW coefficient is  $S_{BGW} = 1.15 \times 10^{-18} \text{ eV.m}^2$  and the intrinsic bandgap (depends only on the band structure) is  $E_g^{int} = 3.15 \text{ eV}$  [23]. Thus, the optically measured band gap ( $E_g$ ) is related to the Moss-Burstein energy ( $\Delta E_g^{BM}$ ) shift by:  $\Delta E_g^{BM} = E_g - 3.15 \text{ eV}$ , for samples controlled by B-M mechanism.

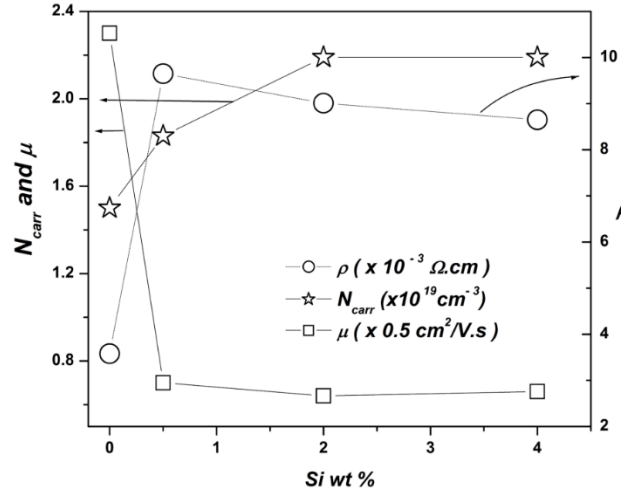


Fig. 4. Conduction parameters, resistivity ( $\rho$ ), mobility ( $\mu$ ), and carrier concentration ( $N_{carr}$ ) extracted from optical data of hydrogenated pristine and Si-incorporated ZnO thin films.

Therefore, the measured shifts,  $\Delta E_g^{BM} \sim 0.07 \text{ eV}$ ,  $0.08 \text{ eV}$ ,  $0.09 \text{ eV}$  and  $0.09 \text{ eV}$  were matching to the values of  $N_{carr}$ ;  $1.5 \times 10^{19} \text{ cm}^{-3}$ ,  $1.8 \times 10^{19} \text{ cm}^{-3}$ ,  $2.2 \times 10^{19} \text{ cm}^{-3}$  and  $2.2 \times 10^{19} \text{ cm}^{-3}$  for ZnO, ZnOSi-1, ZnOSi-2, and ZnOSi-3 films, respectively. The concentration of carriers in pristine ZnO film of the present work ( $1.50 \times 10^{19} \text{ cm}^{-3}$ ) is close to the result  $\sim 10^{19} \text{ cm}^{-3}$  found in ref. [29] and  $2.56 \times 10^{18} \text{ cm}^{-3}$  obtained in ref. [30]. Such carrier concentration is attributed to the point defects, like O-vacancies, present in the ZnO film sample that depend on the preparation conditions, due to which different results were found in the literature. The carrier concentration increased with increasing of Si% inclusion attaining the highest value ( $\sim 2.2 \times 10^{19} \text{ cm}^{-3}$ ) for  $\sim 4.7 - 9.3 \text{ at\%}$  Si content. The increase of carrier concentration with Si doping level was also observed in ref.[31]. The given results in refs. [15,31,32] showed that the carrier concentrations of Si-doped ZnO were in the range  $10^{18} - 10^{20} \text{ cm}^{-3}$ , which agree with the present results, although different methods of preparation were used. The resistivity ( $\rho$ ) of a film can be estimated by [33];  $\rho = (2\epsilon_0 c)^{-1} (R^{-0.5} - 1) \cdot d$ , where, d is the film thickness,  $\epsilon_0 c = 1/376 \text{ } \Omega^{-1}$ , R is the high-wavelength reflectance in the near-infrared (NIR) region where the spectral R is almost constant at  $\lambda \sim 1000 \text{ nm}$  in Fig.2a-b. The resistivity ( $\rho$ ) is related to the carrier concentration ( $N_{carr}$ ) and mobility ( $\mu$ ) by:  $\rho^{-1} = N_{carr} e \mu$ . Thus,  $\mu$  was calculated and presented in Table 2. Fig. 4 demonstrates graphically the variation of the electrical parameters extracted from optical measurements.

Table 2. Conduction parameters, CPs [resistivity ( $\rho$ ), carrier concentration ( $N_{carr}$ ), and carrier mobility ( $\mu$ )] extracted from the optical data

| Sample    | $\rho (10^{-3} \Omega cm)$ | $N_{carr} (10^{19} cm^{-3})$ | $\mu (cm^2/V.s)$ |
|-----------|----------------------------|------------------------------|------------------|
| ZnO-H     | 3.6                        | 1.5                          | 1.15             |
| ZnSiO-1-H | 9.6                        | 1.83                         | 0.35             |
| ZnSiO-2-H | 9.0                        | 2.2                          | 0.32             |
| ZnSiO-3-H | 8.6                        | 2.2                          | 0.33             |
| ZnSiO-4-H | 8.5                        | ---                          | ---              |

For undoped ZnO-H nanocrystallite film, the mobility ( $1.15 \text{ cm}^2/\text{V.s}$ ) was small due to the high carrier concentration. The present-work mobility,  $\mu$  is close to those previously obtained by using Hall measurements, which was around  $\sim 1.0 \text{ cm}^2/\text{V.s}$  [34,35]. The variations of the conduction parameters shown in Table 2 and Fig.5, describe the style of Si ions incorporation in ZnO lattice. For the lowest ( $\sim 1.2\text{at}\%$ ) Si incorporation level, the resistivity greatly increased by  $\sim 2.7$  times. This result can be attributed to the occupation of Si impurity ions the interstitial positions and accumulation at the crystallite boundaries, which enhanced the carrier scattering leading to increase  $\rho$  and decrease  $\mu$ .

The Haacke figure of merit (FOM) of TCO is defined as  $FOM = T^{10}/R_{sheet}$ , where  $T$  is the transmittance of the transparent region and  $R_{sheet}$  is the sheet resistance [36]. The calculated FOMs of the present samples were ;  $\sim 0.6 \times 10^{-3} \Omega^{-1}$ ,  $1.5 \times 10^{-3} \Omega^{-1}$ ,  $1.7 \times 10^{-3} \Omega^{-1}$ ,  $1.9 \times 10^{-3} \Omega^{-1}$ ,  $2.1 \times 10^{-3} \Omega^{-1}$  for ZnO, ZnOSi-1, ZnOSi-2, ZnOSi-3, and ZnOSi-4, respectively. Thus, the FOM increased with the increase of Si content in ZnO film.

## 5. Conclusions

Nano-crystallite ZnO:Si thin films were deposited by the evaporation technique using carbon powder as TRA. It was observed that the incorporated Si ion species in ZnO lattice could distort the crystalline structure. Moreover, the hydrogenation of the samples assists the Si species content to distort the crystalline lattice of ZnO starting with  $4.7\text{at}\%$  Si concentration. The bandgap was slightly blue-shifted due to the Si incorporation, which is attributed to the M-B effect. Thus, the carrier concentrations of the samples were calculated optically. For undoped ZnO, the carrier density was estimated to be  $\sim 10^{19} \text{ cm}^{-3}$ . The little increase in carrier concentration showed that dopant Si ions could not be in  $4+$  oxidation state. The resistivity and mobility were also calculated by using the measured optical data. The variation in conduction parameters with Si doping can be explained by the style of Si incorporation in ZnO lattice.

## References

- [1] T. L. Phan, R. Vincent, D. Cherns, N. X. Nghia, V. V. Ursaki, Nanotechnology **19**, 475702 (2008).
- [2] A. Balhamri, A. Deraoui, Y. Bahou, M. Rattal,

- Az. Mouhsen, M. Harmouchi, A. Tabyaoui, E. M. Oualim, International Journal of Thin Film Science and Technology **4**(3), 205 (2015).
- [3] K. Samanta, P. Bhattacharya, R. Katiyar, W. Iwamoto, P. Pagliuso C. Rettori, Phys. Rev. B **73**, 245213 (2006).
- [4] Anderson Janotti, Chris G Van de Walle, Rep. Prog. Phys. **72**, 126501 (2009).
- [5] K. Ellmer, A. Klein, B. Rech (eds.), Transparent Conductive Zinc Oxide-Basics and Applications in Thin Film Solar Cells, Series: Springer Series in Materials Science, **104**, 2008, Germany.
- [6] T. Moriga, Y. Hayashi, K. Kondo, Y. Nishimura, K. Murai, I. Nakadayashi, J. Vac. Sci. Technol. A **22**, 1705 (2004).
- [7] V. N. Zhitomirsky, E. Cetinorgu, R. L. Boxman, S. Goldsmith, Thin Solid Films **516**, 5079 (2008).
- [8] B. D. Ahn, S. H. Oh, C. H. Lee, G. H. Kim, H. J. Kim S. Y. Lee, J. Cryst. Growth **309**, 128 (2007).
- [9] H. Huang, Y. Ou, S. Xu, G. Fang, M. Li, X. Z. Zhao, Appl. Surf. Sci. **254**, 2013 (2008).
- [10] H. Lv, D. D. Sang, H. D. Li, X. B. Du, D. M. Li, G. T. Zou, Nanoscale Res. Lett. **5**, 620 (2010).
- [11] C. X. Xu, X. W. Sun, Z. L. Dong, M. B. Yu, Appl. Phys. Lett. **85**, 3878 (2004).
- [12] B. D. Yao, Y. F. Chan, N. Wang, Appl. Phys. Lett. **81**, (7572002).
- [13] B. D. Cullity, S. R. Stock, Elements of X-Ray Diffraction. 3rd ed. 2001: Prentice Hall. P.102.
- [14] Nessa Fereshteh Saniee, Structural, Electrical and Optical Properties of Transparent Conducting Si-doped ZnO Thin Films Grown by Pulsed Laser Deposition, A thesis submitted to the University of Birmingham For the degree of master of philosophy, University of Birmingham, 5 (2009).
- [15] J. Clatot, G. Campet, A. Zeinert, C. Labrugere, M. Nistor, A. Rougier, Solar Energy Materials & Solar Cells **95**, 2357 (2011)
- [16] J. Clatot, G. Campet, A. Zeinert, C. Labrugere, A. Rougier, Applied Surface Science **257**, 5181 (2011).
- [17] R. D. Shannon, Acta Crystallogr. A **32**, 751 (1976).
- [18] A. K. Das, P. Misra, L.M. Kukreja, Journal of Physics D: Applied Physics **42**, 165405 (2009).
- [19] Y. G. Wang, S. P. Lau, H. W. Lee, S.F Yu, B. K Tay, X. H. Zhang, K. Y. Tse, H. H. Hng, J. Appl. Phys. **94**, 1597 (2003).
- [20] Abdel-Sattar Gadallah, M. M. El-Nahass, Adv. Condens. Matter Phys. **2013**, 234546 (2013).
- [21] M. Durr, U. Hofer, Surface Science Reports **61**, 465 (2006).
- [22] J. Tauc, F. Abelesn, Optical Properties of Solids, Amsterdam, Holland: North Holland, 1969.
- [23] V. Srikant, D. R. Clarke, J. Appl. Phys. **83**, 5447 (1998).
- [24] M. F. Malek, M. H. Mamat, M. Z. Musa, Z. Khusaimi, M. Z. Sahdan, A. B. Suriani, A. Ishak, I. Saurdi, S. A. Rahman, M. Rusop, J. Alloys Comps. **610**, 575 (2014).
- [25] Sergej Repp and Emre Erdem, Spectrochim. Acta

- Part A: Molecular and Biomolecular Spectroscopy **152**, 637 (2016).
- [26] L. A. Patil, A. R. Bari, M. D. Shinde, Vinita Deo, M. P. Kaushik, *Adv. Powder Technology* **22**, 722 (2011).
- [27] Dengyuan Song, *Appl. Surf. Sci.* **254**, 4171 (2008).
- [28] J. I. Pankove, *Optical Processes in Semiconductors*, Dover Publications, Inc., New York, 36 (1975).
- [29] C. Maragliano, S. Lilliu, M. S. Dahlem, M. Chiesa, T. Souier, M. Stefancich, *Scientific Reports* **4**, 4203(2014).
- [30] K. G. Saw, N. M. Aznan, F. K. Yam, S. S. Ng, S. Y. Pung, *PLoS ONE* **10**(10), e0141180 (2015).
- [31] J. T. Luo, X.Y. Zhu, G. Chen, F. Zeng, F. Pan, *Applied Surface Science* **258**, 2177 (2012).
- [32] Nazanin Rashidi, Vladimir L. Kuznetsov, Jonathan R. Dilworth, Michael Pepper, Peter J. Dobson, Peter P. Edwards, *J. Mater. Chem. C* **1**, 6960 (2013).
- [33] H. L. Hartnagel, A. L. Dawar, A. K. Jain, C. Jagadish, *Semiconducting Transparent Thin Films*, Institute of Publishing Bristol and Philadelphia, UK, Institute of Physics, London, 248 (1995).
- [34] K. Meziane, A. El Hichou, A. El Hamidi, M. Mansori, A. Liba, A. Almaggoussi, *Superlattices and Microstructures* **93**, 297 (2016).
- [35] Arindam Mallick and Durga Basak, *Progress in Materials Science* **96**, 86 (2018).
- [36] A. E. Hassanien, H. M. Hashem, G. Kamel, S. Soltan, A. M. Moustafa, M. Hammam, A. A. Ramadan, *International Journal of Thin Film Science and Technology* **5**, 55 (2016).

---

\* Corresponding author: adakhil@uob.edu.bh